THE PENNSYLVANIA STATE UNIVERSITY
SCHREYER HONORS COLLEGE

DEPARTMENT OF AEROSPACE ENGINEERING

Investigation of the Relative Motion Between Spacecraft on Different Hyperbolic Trajectories

CLIFFORD STUECK
SPRING 2022

A thesis
submitted in partial fulfillment
of the requirements
for a baccalaureate degree
in Aerospace Engineering
with honors in Aerospace Engineering

Reviewed and approved* by the following:

Robert G. Melton
Professor of Aerospace Engineering
Thesis Supervisor

Philip J. Morris
Boeing, A.D. Welliver Professor of Aerospace Engineering
Honors Adviser

* Electronic approvals are on file.

ABSTRACT

The purpose of this research is to assess the effects of differences in position, inclination, and right ascension of the ascending node (RAAN) when applied to multiple spacecraft on different hyperbolic orbits. The rationale for conducting this work is to understand if the suggested model can prove useful for interplanetary missions involving two or more spacecraft on hyperbolic paths with respect to an object of interest. As an example, this could mean collecting sensor data from separate vehicles that could then be combined to form a distributed sensor.

The range and range-rate between spacecraft pairs were compared to observe how different orbits and initial conditions could prove useful in minimizing the average range and range-rate. The study revealed that a change in inclination presented the smallest range whereas a change in RAAN was able to limit the range-rate between the spacecraft on different orbits. However, if two spacecraft are on the same orbit, changes to the RAAN and inclination have practically no impact on the range and range rate of the spacecraft pair.

A future study will apply the second order solution of the relative-motion model to hyperbolic paths to examine if an improvement in accuracy can be made in determining the coordinates of the spacecraft, but with lower computational burden. An optimizer will also be implemented for minimizing the average range and range-rate in order to determine a method for ways in which multiple spacecraft on different orbits can find a time to communicate with each other while they move together around a planet.

TABLE OF CONTENTS

LIST OF FIGURES

LIST OF TABLES

ACKNOWLEDGEMENTS

I would like to thank my thesis advisor, Dr. Melton, for his indispensable support in establishing and perfecting this thesis. His knowledge of the topic has enabled me to develop a much deeper understanding of orbital mechanics and his suggestions and ideas have always left me wondering what else could be included and done to better my work.

I would also like to thank my honors advisor, Dr. Morris, for helping me with many of the major decisions I have been faced with while at Penn State. He has always been a great resource for me and guided me towards many opportunities I don't think I would have been able to find or learn about without his help.

Finally, I would like to thank my family for the all the support they have given me and their never-ending encouragement to study Aerospace Engineering. They have believed in me from the beginning and taught me that even when things get hard there is always a light at the end of the tunnel.

This thesis is dedicated to the ones who stood by my side and believed in me even when nobody else did. Thank you all for being a part of my story.

NOMENCLATURE

G	=	Universal Gravitational Constant $\left[\mathrm{N}\left(\frac{\mathrm{m}}{\mathrm{kg}}\right)^2\right]$
m	=	Mass [kg]
μ	=	Standard Gravitational Parameter $\left[\frac{\mathrm{km}^3}{\mathrm{s}^2}\right]$ or $\left[\frac{\mathrm{LU}^3}{\mathrm{TU}^2}\right]$
a	=	Semi-Major Axis [km] or [LU]
r_p	=	Radius of Periapsis [km] or [LU]
p	=	Semi-Latus Rectum [km] or [LU]
e	=	Eccentricity
h	=	Specific Angular Momentum $\left[\frac{\mathrm{km}^2}{\mathrm{s}}\right]$ or $\left[\frac{\mathrm{LU}^2}{\mathrm{TU}}\right]$
ε	=	Specific Orbital Energy $\left[\frac{\mathrm{km}^2}{\mathrm{s}^2}\right]$ or $\left[\frac{\mathrm{LU}^2}{\mathrm{TU}^2}\right]$
Δ	=	Change in Element
θ	=	True Anomaly [radians]
Ω	=	Right Ascension of the Ascending Node [radians]
ω	=	Argument of Periapsis [radians]
i	=	Inclination [radians]
$\vec{r}$	=	Position Vector [km] or [LU]
$\vec{v}$	=	Velocity Vector $\left[\frac{\mathrm{km}}{\mathrm{s}}\right]$ or $\left[\frac{\mathrm{LU}}{\mathrm{TU}}\right]$
D	=	Relative Distance (Range) [km] or [LU]
$\frac{dD}{dt}$	=	Relative Rate of Change in Distance (Range-Rate) $\left[\frac{\mathrm{km}}{\mathrm{s}}\right]$ or $\left[\frac{\mathrm{LU}}{\mathrm{TU}}\right]$
LU	=	Canonical Distance Unit
TU	=	Canonical Time Unit
$\hat{X}, \hat{Y}, \hat{Z}$	=	Cartesian Coordinate Frame Unit Vectors
$\hat{I}, \hat{J}, \hat{K}$	=	Earth-Centered Inertial Coordinate Frame Unit Vectors

Chapter 1

Introduction

Remote sensing using satellites has been successfully employed in many space missions since the 1960's. Examples include routine meteorological measurements, climate-change observations, Earth-resource assessments, and surface-shape measurements for terrain-mapping. A single large-aperture sensor, such as a telescope, can produce higher resolution images than one with a smaller aperture, but large-aperture sensors can present difficult mechanical challenges (the sensor often has a diameter that exceeds that of the satellite). An alternative approach is to use several smaller-aperture sensors that work simultaneously and whose data are merged to produce measurements or images of a nearly equivalent quality to that of a large-aperture sensor. This approach is called distributed sensing, and it has been used successfully on Earth-orbiting satellites as observed in papers by Barnhart et al [1], and Elderman and Gurfil [2].

This thesis considers the concept of using several satellites as a distributed sensor as they fly by a planet. A principal requirement is that the relative distances between pairs of satellites remain relatively constant (or at least change slowly during the measurements). Flyby maneuvers occur on hyperbolic trajectories, and these form an important component for studying the feasibility of this distributed-sensing concept.

Conventionally, hyperbolic orbits are also considered to be escape trajectories because they have a positive energy, enabling them to carry a spacecraft out of the gravitational sphere of influence of the body they are orbiting. Hyperbolic trajectories have many uses, the principal of

which are for flybys of objects of interest such as planets or moons, for observation and gravitational assists to increase or decrease a spacecraft's speed or redirect its path. However, in more recent years, studies have been conducted to show how hyperbolic trajectories can be used in conjunction with multiple spacecraft to perform actions around or near celestial bodies. These actions can include satellites acting to relay planetary information, spacecraft coming together to form a distributed sensor, or even spacecraft on different hyperbolic trajectories being used to conduct a survey of the entire landscape of a body. Scientists have coined the term "swarm" theory for the study of this type of collective motion [3].

As will be discussed in Chapter 2, a spacecraft's position on a hyperbolic trajectory cannot be determined as a closed-form function of time. Therefore, numerical integration of the equations of motion will be used to calculate the distances and their rates of change for spacecraft on hyperbolic trajectories during planetary flybys.

Chapter 2

Problem Statement

Orbital mechanics involves finding ways to study objects in space moving under the influence of forces such as gravity, atmospheric drag, thrust, etc. To study the relative position of spacecraft and speed between two or more spacecraft on hyperbolic paths, an analysis of trajectories with differing orbital elements is explored. The ultimate goal is to consider what happens if three or more hyperbolic paths with the same eccentricity, oriented differently, are compared. As an example, this could include studying the average range and the range-rate over some interval of time, as well as adjusting the orbital elements to try and minimize the rate and the range-rate.

2.1 Hyperbolic Trajectories

Hyperbolic trajectories can be identified by their geometric qualities and dynamic behavior with the idea being that a body traveling along this trajectory will coast towards infinity, settling to a final non-zero (so-called excess) velocity relative to the central body. Like an elliptical orbit, a hyperbolic trajectory for a given system can be defined by its semi major axis and eccentricity. The following table shows how a hyperbolic trajectory differs from other conic orbits.

Table 1. Conic Orbit Definitions

Conic	**Eccentricity (e)**	**Semi-Major Axis (a)**	**Energy (Ɛ)**
Circle	e = 0	a > 0	Ɛ < 0
Ellipse	0 < e < 1	a > 0	Ɛ < 0
Parabola	e = 1	a → ∞	Ɛ = 0
Hyperbola	e > 1	a < 0	Ɛ > 0

An example of how a hyperbola is geometrically represented is shown in Fig. 1.

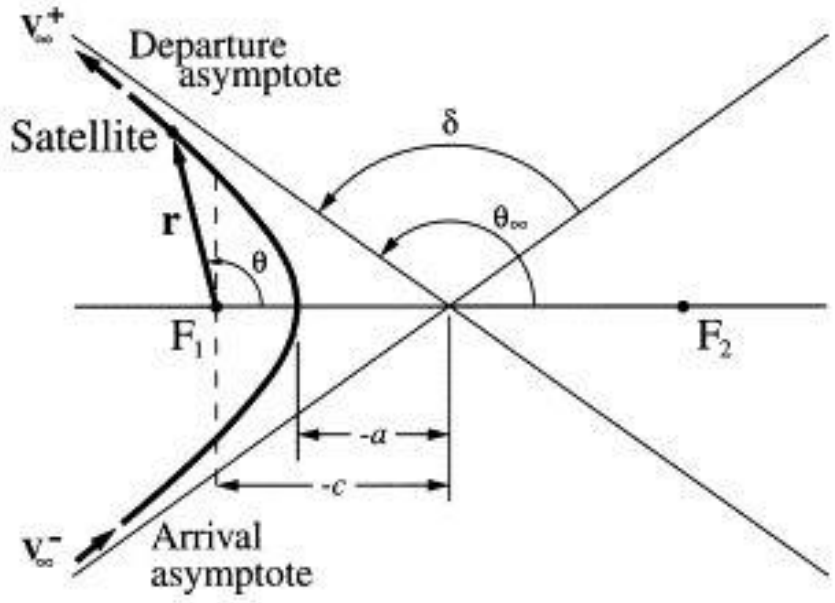

Figure 1. Geometric Significance of a Hyperbolic Trajectory [6]

where F is the focus of the conic, r is the position vector of the spacecraft, θ describes where the spacecraft is located on the orbit, V_∞ represents the hyperbolic excess velocity with the positive superscript denoting departure and the minus sign denoting arrival, δ is the angle between the departure and the arrival asymptotes, and θ_∞ is the true anomaly as the trajectory

goes to infinity. The quantity a is used to represent the semi-major axis of the orbit. It should also be noted that in Fig. 1, -c = -ae where e is the eccentricity of the hyperbola.

2.2 Hyperbolic Time Equation

In a typical problem where the position of a spacecraft on a hyperbolic trajectory at a given time is desired, the hyperbolic anomaly (H) can be calculated using the relationship.

$$\sqrt{\frac{\mu}{-(a)^3}}(t - t_o) = e \sinh H - H \tag{1}$$

where μ is the gravitational parameter of the celestial body, a is the semi-major axis of the orbit, and t_o is the epoch time or a reference time to which the orbital elements are referred. The relationship between H and the physically significant angle θ is

$$\tan\frac{\theta}{2} = \sqrt{\frac{e+1}{e-1}}\tanh\frac{H}{2} \tag{2}$$

However, there is no closed-form solution for H in Eq. (1). This means that in order to compute the position of the spacecraft on a hyperbolic trajectory for a given time, t, one must either solve Eq. (1) by numerical iteration or employ numerical integration of the dynamic equations of motion.

For the problem under consideration here, where the positions of multiple spacecraft at many different times must be determined, numerical integration is the more efficient method.

2.3 Numerical Integration

The utilization of the ODE45 Runge-Kutta method is pertinent to conducting analysis on multiple hyperbolic trajectories at the same time. ODE45 is a built-in function in MATLAB based on an explicit Runge-Kutta (4, 5) formula that computes the position at the current time using only the position from the previous time step and derivative information from the equations of motion [12]. ODE45 will be used to simultaneously integrate multiple trajectories in order to compare the relative distance (range) and rate of change in distance (range-rate) of satellites on different three-dimensional hyperbolic trajectories.

2.4 Equations of Motion

In order to study and compare the change in distance and rate at which that same distance is changing between vehicles on hyperbolic trajectories, the equations of motion (EOMs) need to be derived and interpreted so that a solution can be integrated and examined.

The equations of motion were derived in both polar and cartesian coordinates so that the optimum approach could be taken with the study. To compute the polar equations in the inertial frame, the transport theorem was applied to a position vector, $\vec{r}$.

$$\frac{d^2\vec{r}^{\,I}}{dt^2} = \frac{d^2\vec{r}^{\,O}}{dt^2} + \frac{d\vec{\omega}^{\,O}}{dt} \times \vec{r} \; + 2\vec{\omega} \times \frac{\mathrm{d}\vec{r}^{\,O}}{dt} + \vec{\omega} \times (\vec{\omega} \times \vec{r}) = \frac{-\mu \hat{\imath}_r}{r^2} \tag{3}$$

where the subscripts I and O denote differentiation with respect to an inertial frame I and a frame O that is rotating with angular velocity, $\vec{\omega}$, with respect to frame I.

$$\vec{\omega} = \dot{\theta}\vec{\imath}_z \tag{4}$$

$$\frac{d^2\vec{r}^{\,O}}{dt^2} = \ddot{r}\hat{\imath}_r \tag{5}$$

$$\frac{d\vec{\omega}^{\,O}}{dt} \times \vec{r} = r\ddot{\theta}\hat{\imath}_\theta \tag{6}$$

$$2\vec{\omega} \times \frac{\mathrm{d}\vec{\mathrm{r}}^{\,O}}{dt} = 2\dot{r}\dot{\theta}\hat{\imath}_\theta \tag{7}$$

and

$$\vec{\omega} \times (\vec{\omega} \times \vec{r}) = -r\dot{\theta}^2\hat{\imath}_r \tag{8}$$

can be used to simplify Eqs. (3-8),

$$\frac{d^2\vec{r}^{\,\mathrm{I}}}{dt^2} = \ddot{r}\hat{\imath}_r + r\ddot{\theta}\hat{\imath}_\theta + 2\dot{r}\dot{\theta}\hat{\imath}_\theta - r\dot{\theta}^2\hat{\imath}_r = \frac{-\mu\hat{\imath}_r}{r^2} \tag{9}$$

Separating Eq. (9) into $\hat{\imath}_r$ and $\hat{\imath}_\theta$ components, the second order equation can be put into state variable form where

$$x_1 = r \qquad x_2 = \dot{r} \qquad x_3 = \theta \qquad x_4 = \dot{\theta} \tag{10}$$

The state equations can finally be derived by taking the derivative of the state variables

$$\dot{x}_1 = x_2 \tag{11a}$$

$$\dot{x}_2 = x_1 x_4^2 - \frac{\mu}{x_1^2} \tag{1b}$$

$$\dot{x}_3 = x_4 \tag{11c}$$

$$\dot{x}_4 = \frac{-x_2 x_4}{x_1} \tag{11d}$$

Upon testing the polar EOMs with e = 1.5, r_p = 1.2, and starting at periapsis, the following graph was created.

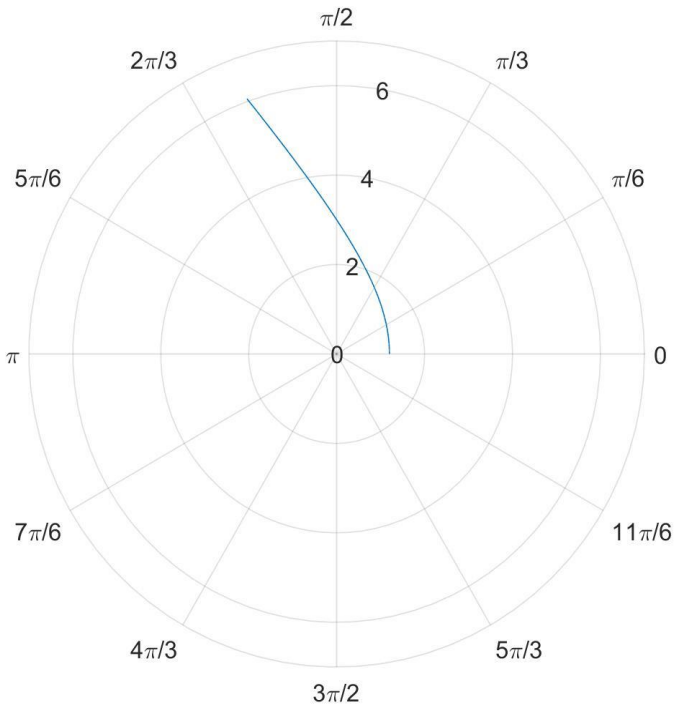

Figure 2. Polar Plot for r_p = 1.2 and e = 1.5

In a similar fashion, the state equations in cartesian coordinates are also computed. Since

$$\ddot{r} = \ddot{x}\hat{I} + \ddot{y}\hat{J} + \ddot{z}\hat{K} = \frac{-\mu}{r^3}\vec{r} \tag{12}$$

and

$$r = \sqrt{x^2 + y^2 + z^2} \tag{13}$$

The state variable form once again can be set up by equating the components of Eq. (12).

$$x_1 = x \qquad x_2 = \dot{x} \qquad x_3 = y \qquad x_4 = \dot{y} \qquad x_5 = z \qquad x_6 = \dot{z} \tag{14}$$

where the state equations can be calculated by taking the derivative of the state variables.

$$\dot{x}_1 = x_2 \tag{15a}$$

$$\dot{x}_2 = -\frac{\mu x_1}{(x_1^2 + x_3^2 + x_5^2)^{\frac{3}{2}}} \tag{15b}$$

$$\dot{x}_3 = x_4 \tag{15c}$$

$$\dot{x}_2 = -\frac{\mu x_3}{(x_1^2 + x_3^2 + x_5^2)^{\frac{3}{2}}} \tag{15d}$$

$$\dot{x}_5 = x_6 \tag{15e}$$

$$\dot{x}_2 = -\frac{\mu x_5}{(x_1^2 + x_3^2 + x_5^2)^{\frac{3}{2}}} \tag{15f}$$

which yields the exact same graph as in Fig. 1, but in the cartesian frame of reference as seen in Fig. 3.

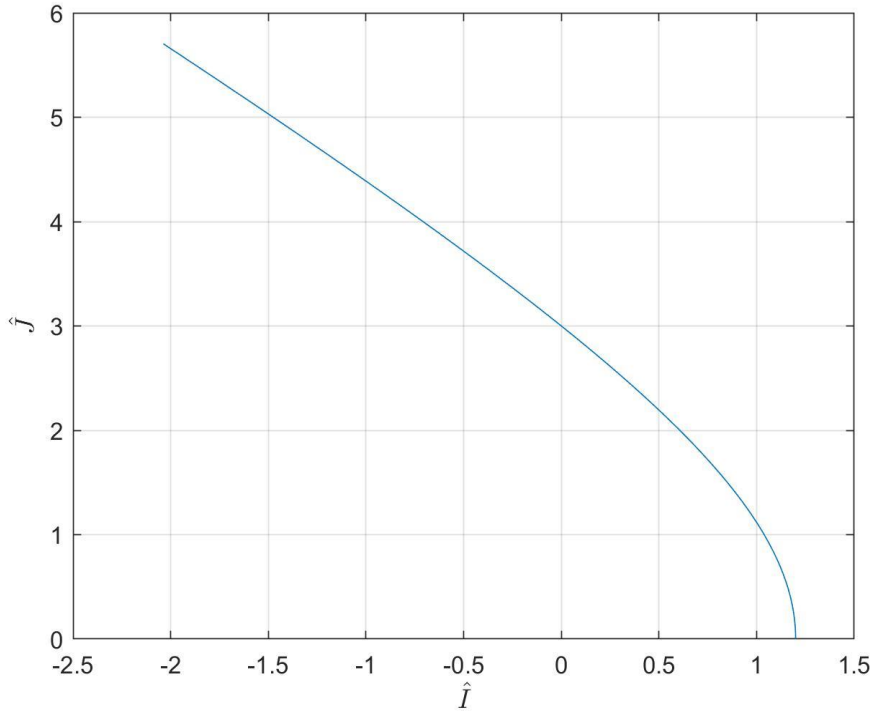

Figure 3. Cartesian Plot for r_p = 1.2 and e = 1.5

The polar and cartesian state vectors were compared and analyzed using an initial evaluation of hyperbolic orbit definition. Ultimately, it was determined that while in the short-term polar coordinates were easier to use and manipulate, it would be difficult to transform them into orbital elements whereas cartesian coordinates could be used not only to easily calculate the orbital elements, but also to directly relate them to the Earth Centered Inertial (ECI) coordinate frame. This would ensure that all subsequent calculations related to relative distance and rate of distance could be compared.

2.5 Perifocal Coordinate Frame

Since a perifocal coordinate can define an orbit in two dimensions based only on spacecraft position (r, θ), eccentricity (e), and semi-major axis (a), this is the path selected. It is much simpler to use as an intermediate coordinate system to define the different hyperbolic trajectories than trying to determine the three-dimensional properties of the orbit immediately.

In a perifocal coordinate frame, the $\hat{P}$ unit vector points to the periapsis (x-direction) while the $\hat{Q}$ unit vector points in the direction of the semi-latus rectum (y-direction). This enables the x and y coordinates to easily be computed using the $\hat{P}$ and $\hat{Q}$ directions of the perifocal coordinate frame.

$$\vec{r} = x\hat{X} + y\hat{Y} = rcos\theta\hat{P} + rsin\theta\hat{Q} \tag{16}$$

Since the magnitude of the position vector is also defined as

$$r = \frac{a(1-e^2)}{1+ecos\theta} = \frac{p}{1+ecos\theta} \tag{17}$$

Eq. (16) can be simplified to include the known parameters a, e, and θ

$$x = \frac{p}{1 + ecos\theta} cos\theta \tag{18}$$

$$y = \frac{p}{1 + ecos\theta} sin\theta \tag{19}$$

The x and y components of velocity can also be determined by utilizing the following derivation of the orbit equation and $\dot{\theta}$ equation

$$\dot{r} = \frac{\mu}{h} esin\theta \tag{20}$$

$$\dot{\theta} = \frac{h}{r^2} \tag{21}$$

where h is the specific angular momentum of the orbital body and μ is the gravitational parameter of the focus. The velocity in the perifocal frame is established to be

$$\vec{v} = \dot{x}\hat{I} + \dot{y}\hat{J} = (\dot{r}cos\theta - r\dot{\theta}sin\theta)\hat{P} + \left(\dot{r}sin\theta + r\dot{\theta}cos\theta\right)\hat{Q} \tag{22}$$

which can be simplified with Eqs. (20-21) to

$$\dot{x} = -\frac{\mu}{h} sin\theta \tag{23}$$

$$\dot{y} = \frac{\mu}{h}(e + cos\theta) \tag{24}$$

Thus, Eqs. (18-24) could all be used to determine the two-dimensional position and velocity of a spacecraft in perifocal coordinates.

2.6 ECI Frame Direction Cosine Matrix

To add three-dimensional properties to the hyperbolic trajectories, a direction cosine matrix (DCM) was constructed using orbital elements. This involved rotating the inertial reference frame three times to acquire the desired frame. The first rotation being the angle

defined by the right ascension of the ascending node (Ω) about the 3-axis, followed by a rotation about the 1-axis defined by the inclination (i), and the final rotation being once again about the 3-axis at an angle equal to the argument of periapsis (ω). The definitions of the orbital elements are shown below in the following figure.

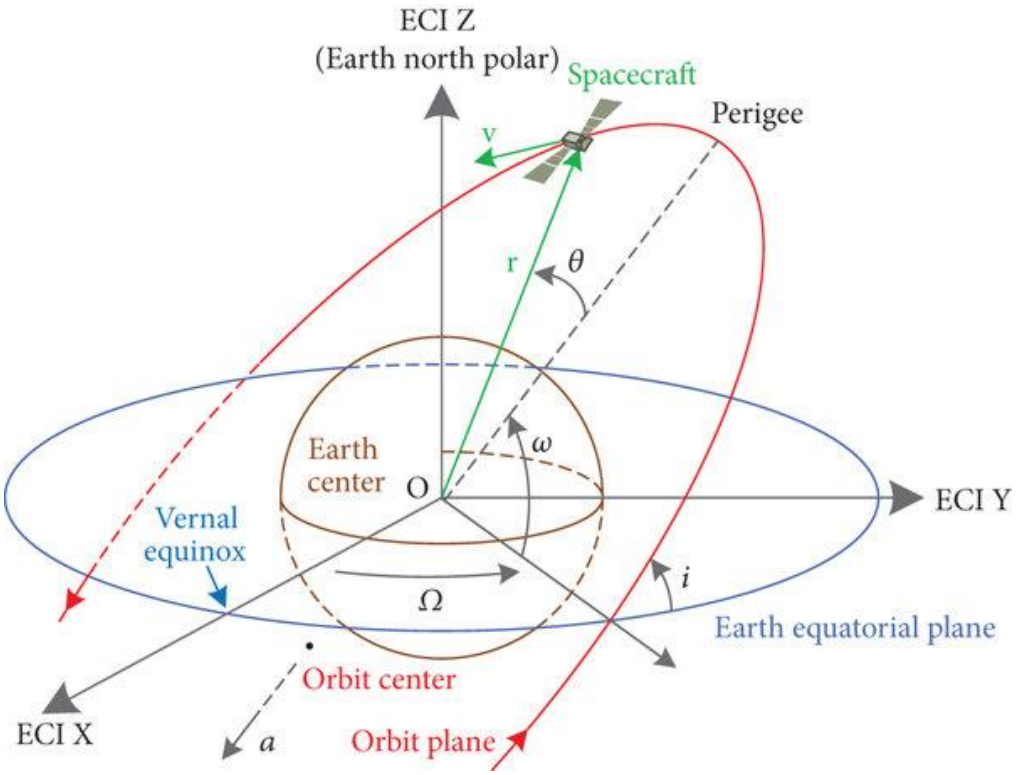

Figure 4. Orbital Element Definitions [5]

The collection of these rotations could then be inverted to produce the DCM from the perifocal coordinate system to the ECI frame as shown below

$$\begin{bmatrix} \hat{I} \\ \hat{J} \\ \hat{K} \end{bmatrix} = \left[\begin{bmatrix} \cos\omega & \sin\omega & 0 \\ -\sin\omega & \cos\omega & 0 \\ 0 & 0 & 1 \end{bmatrix} \begin{bmatrix} 1 & 0 & 0 \\ 0 & \cos i & \sin i \\ 0 & -\sin i & \cos i \end{bmatrix} \begin{bmatrix} \cos\Omega & \sin\Omega & 0 \\ -\sin\Omega & \cos\Omega & 0 \\ 0 & 0 & 1 \end{bmatrix} \right]^{-1} \begin{bmatrix} \hat{X} \\ \hat{Y} \\ \hat{Z} \end{bmatrix} \quad (25)$$

Eq. (25) allows for inclination, argument of periapsis, and right ascension to be considered when determining the hyperbolic trajectories.

Chapter 3

Implementation

In order to perform an analysis between different hyperbolic trajectories, multiple processes needed to be derived. This includes the relative distance between two or more objects on differing hyperbolic orbits, the derivative with respect to time of that distance, and a method of defining orbital elements with respect to the ECI frame. To maintain similarity between the orbits studied, the eccentricity was held constant at 1.5 and the radius of periapsis was always taken to be 1.2 LU. In this section, the calculations and processes used to define these parameters will be discussed.

3.1 Canonical Units

For the purposes of this research and to control the size of the values that would be calculated, a canonical system of units was set up and implemented. In the study, the length unit (LU) was set equal to the value of an arbitrary planet's mean equatorial radius. This meant the planet's radius could be substituted with one LU, and the subsequent calculations would still hold true.

The time unit (TU) was set to the hyperbolic orbital period. Since the eccentricity and radius of periapsis were constant for all studied orbits, the periods of all the orbits also had to be the same. Setting the TU equal to the period of the hyperbolic trajectory allowed for simple integration of the EOMs from 0 to 1 TU.

Finally, the gravitational parameter was assumed to be $\mu = 4\pi^2 \frac{LU^3}{TU^2}$.

3.2 Relative Distance

To compare how one spacecraft moved with respect to another, the distance formula was implemented in cartesian coordinates

$$D = \sqrt{(x_2 - x_1)^2 + (y_2 - y_)^2 + (z_2 - z_1)^2} \tag{26}$$

Since MATLAB was used to numerically integrate the equations of motion over a time period, Eq. (26) had to be applied to every single entry in the arrays, after the integration took place, to find the relative distance between the two vehicles along the entirety of their respective orbits.

3.3 Relative Rate of Change in Distance

The relative rate of change in distance between the entities could be determined by taking the derivative of Eq. (26) with respect to time

$$\frac{dD}{dt} = \frac{(x_2 - x_1)\left(\frac{dx_2}{dt} - \frac{dx_1}{dt}\right) + (y_2 - y_1)\left(\frac{dy_2}{dt} - \frac{dy_1}{dt}\right) + (z_2 - z_1)\left(\frac{dz_2}{dt} - \frac{dz_1}{dt}\right)}{\sqrt{(x_2 - x_1)^2 + (y_2 - y_1)^2 + (z_2 - z_1)^2}} \tag{27}$$

Similar to Eq. (26), Eq. (27) also needed to be applied to every entry in the arrays in order to find the relative change in distance between the two vehicles along the entirety of their respective orbits.

3.4 Average Distance and Average Rate of Distance

For this study, the average distance and average rate of distance were collected by observing one pair of satellites at a time and then reporting the averages for each pair separately.

The averages could then be compared to each other as well as other spacecraft swarms to observe how different inclinations, right ascensions, spacecraft positions, etc. could be affected and manipulated.

For both distance and rate of change in distance, each average could be computed by adding all the values of relative distance and rate of distance and then dividing by the total values present in the array.

$$AVG = \frac{Sum(Values)}{Number\ of\ Values} \tag{26}$$

3.5 Orbital Elements

To aid in making comparisons, the relative distance and relative rate of change in distance were calculated for spacecraft on orbits that varied in three dimensions. Inclination and right ascension of the ascending node (RAAN) were adjusted in Eq. (25) to examine how a change in plane or height could affect relative rate and range-rate. Information on how relative distance and range-rate compared between two dimensions and three dimensions could also be observed and studied by using the orbital elements.

Chapter 4

Results

Following the study, all observations were reported and examined. Multiple graphs were created to visualize and explain how different orbit and position changes could affect relative distance and distance rate, as well as the averages of these same quantities. The term “range” is used to describe the distance between a pair of spacecraft while the “range-rate” is used to detail the time derivative of the range. This section further explores these findings.

4.1 Spacecraft on Same Hyperbola

To explore how spacecraft will move relative to each other on the same hyperbolic trajectory at different starting positions, a simple case was implemented where one vehicle was placed at periapsis while the other was positioned at a starting location of $\theta = 90$ degrees. The resulting trajectories for the time span can be seen in Fig. 3.

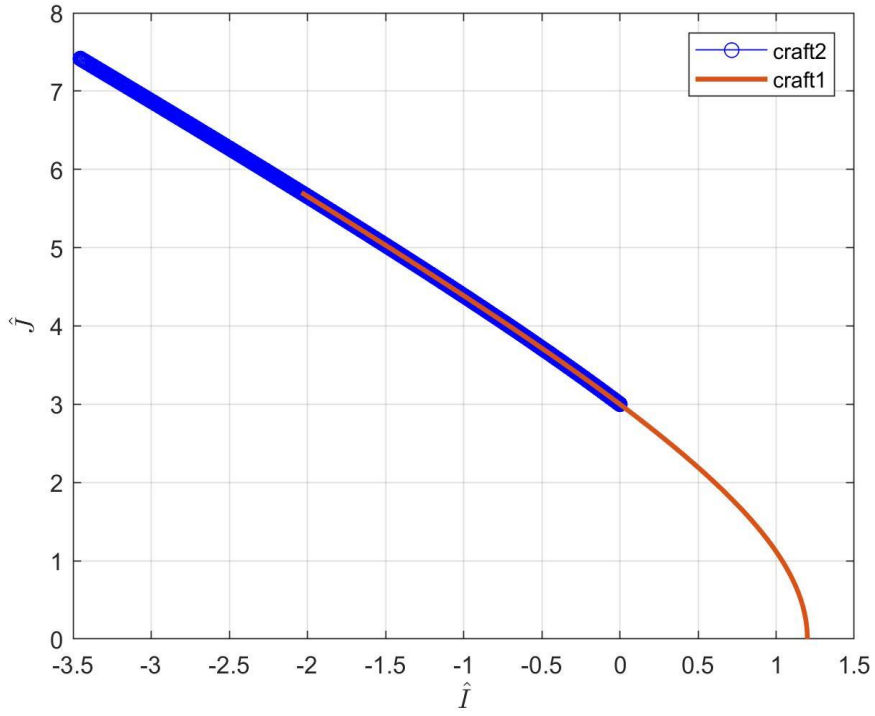

Figure 5. Spacecraft 1 and Spacecraft 2 Trajectories for $\Delta\theta = 90$ degrees

With a similar intention, various other starting locations for the two spacecraft were examined. Using the equations derived previously, an assessment of the relative distance and distance rate was conducted. The results are shown in Fig. 6 and 7 respectively.

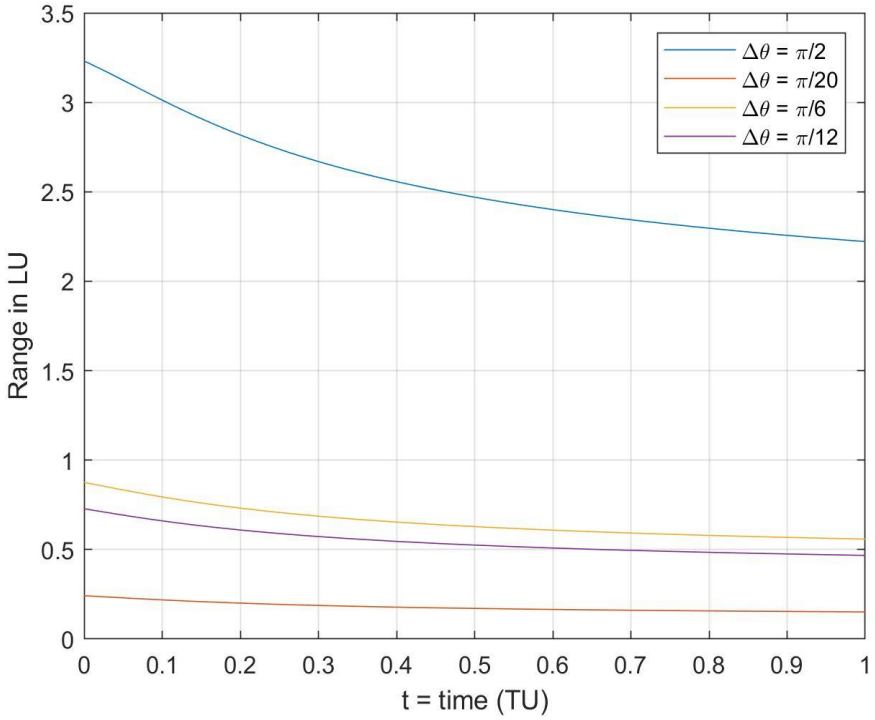

Figure 6. Range of Two Spacecraft with Differing θ

As seen in Fig. 6, it is clear that when two vehicles are on the same hyperbolic trajectory, the range between them appears to decrease as the difference in starting position decreases. Since a larger difference in starting position inherently starts the range at a large value, this result is expected. It is also interesting to note that upon reaching a certain value of time (dependent on the starting positions), the range appears to reach a minimum value.

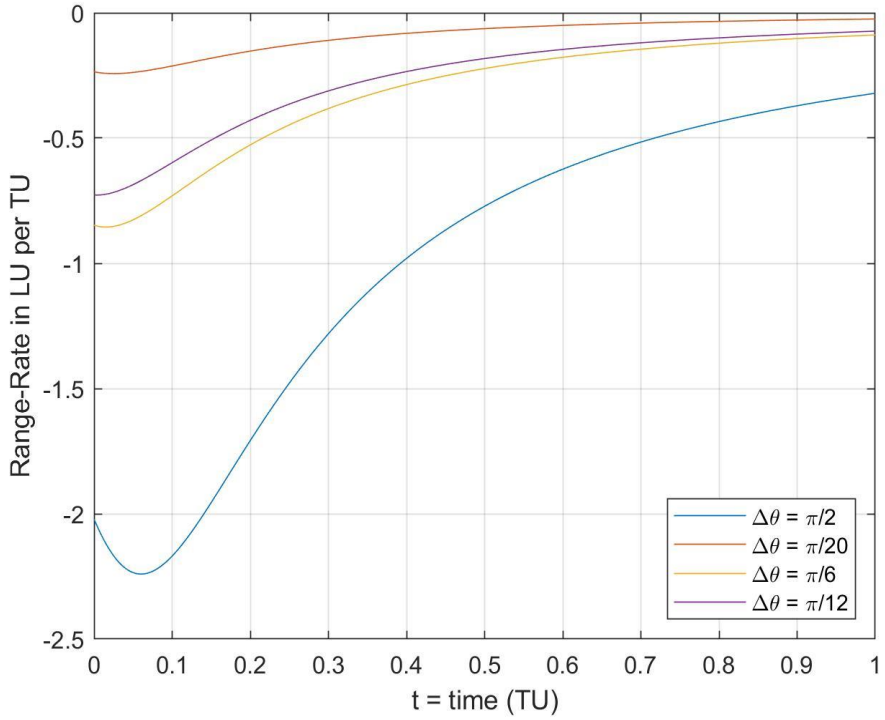

Figure 7. Range-Rate vs. Time for Changing $\Delta\theta$

In Fig. 7, it is interesting to note that the resulting curves from the calculations are mostly similar in magnitude throughout the entirety of the time span. This indicates that while starting positions may impact the starting velocity or how quickly each vehicle accelerates, the resulting range-rate will always eventually follow the same trend.

Each curve also reaches some minimum value before slowly increasing in range-rate to a steady state near 0 LU/TU, which represents the idea that one vehicle is catching up to the other. Since the only difference between the two spacecraft is their difference in starting position, it is possible that this phenomenon is due to there being a certain point along the orbit where the spacecraft are no longer pulling away from each other, enabling a way for the relative velocity

and distance between the spacecraft to become almost constant. This behavior could be exploited to form a distributed sensor when the spacecraft are near this minimum range-rate point.

4.2 Spacecraft at Periapsis of Hyperbolas with Differing Inclination

The next step was to determine how the spacecraft will move relative to each other on hyperbolic trajectories with different inclinations, but with the spacecraft both starting at periapsis. As a visual example, one of the tested cases can be seen in Fig. 8.

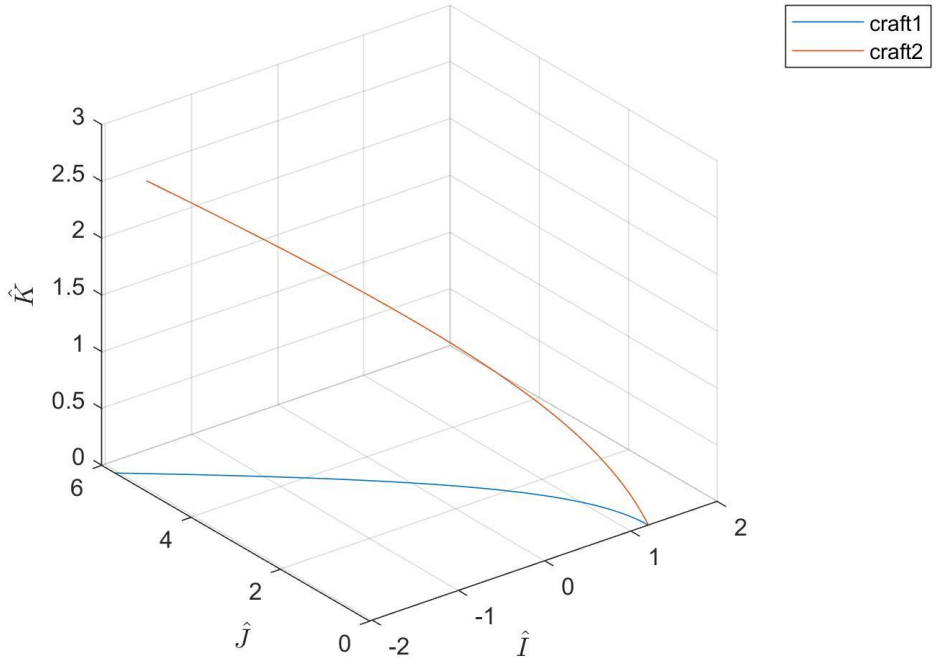

Figure 8. Spacecraft 1 and Spacecraft 2 Trajectories for i = 0 rad and i = 0.5 rad

Even though the spacecraft have the same starting point, it is clear that the range and range-rate will still increase over time due to the constant increase in the $\hat{K}$ direction. This is

documented below in Fig. 9 and 10, which shows how the spacecraft move relative to each other over the time span.

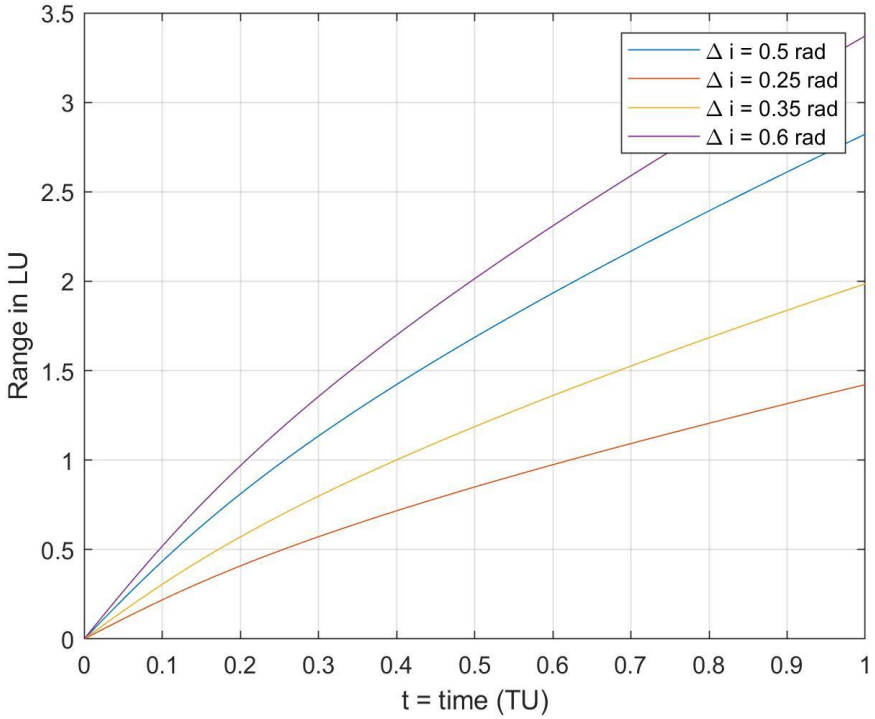

Figure 9. Range vs. Time for Differing Inclination

As a contrast to Fig. 6, the curves in Fig. 9 do not find a steady state at any point along the time span, but instead appear to increase towards infinity. As stated earlier, this is likely due to the constant increase in distance in the $\widehat{K}$ direction. It is also interesting to note that with larger inclination difference between trajectories, comes a larger difference and faster increase in range of the two vehicles.

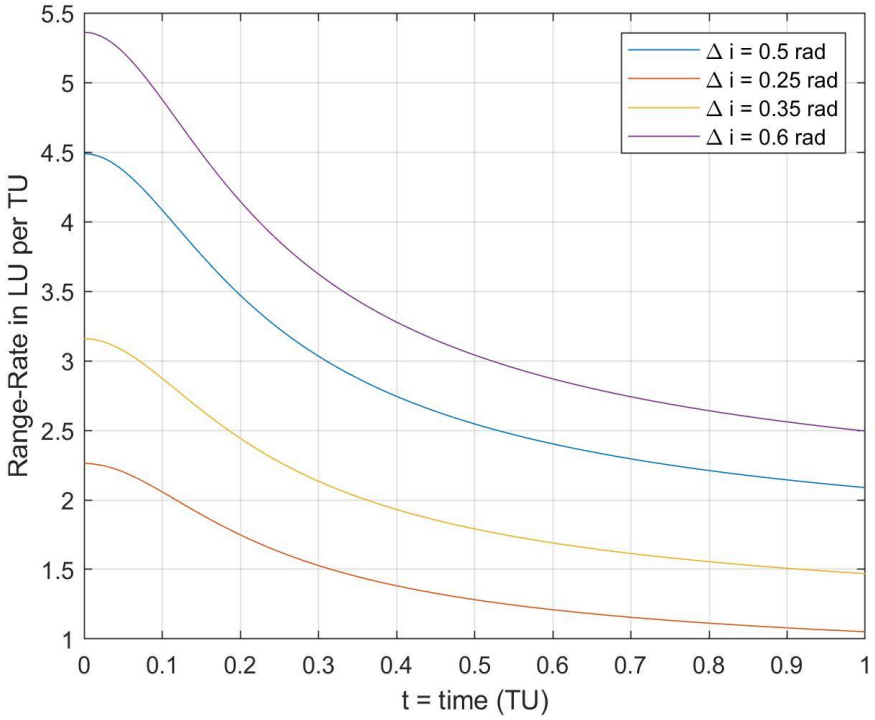

Figure 10. Range-Rate vs. Time for Differing Inclination

Fig. 10 appears to show the relative rate curves coming to a steady state right at the end of the time span. This is an interesting result since in Fig. 9, the curves all increased across the entire time span. It should also be noted that larger values of inclination difference appear to correspond to larger range-rate values. The difference in inclination appears to have larger and smaller values of difference interchanged within starting positions.

4.3 Spacecraft at Periapsis of Hyperbolas with Differing RAAN

After examining how inclination affected range and range-rate, a thorough study into the effects of the RAAN needed to be conducted and compared. The spacecraft were still positioned directly at periapsis to start. As a visual example, one of the tested cases can be seen in Fig. 11.

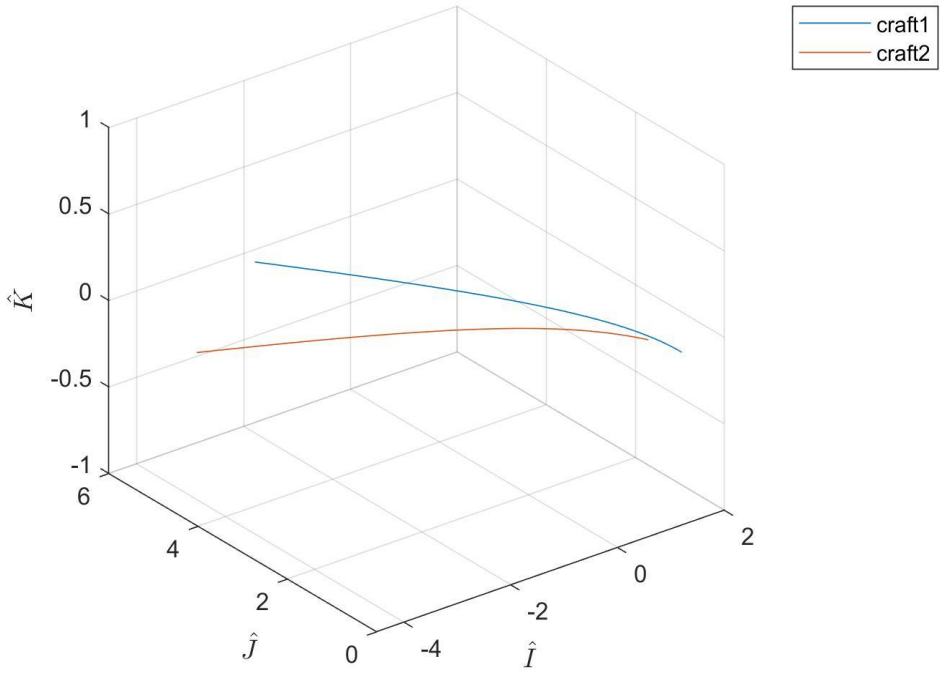

Figure 11. Spacecraft 1 and Spacecraft 2 Trajectories for Ω = 0 rad and Ω = 0.5 rad

A quick survey of Fig. 11 reveals that a difference in RAAN offsets the trajectories. Since inclination is considered to be zero in this portion of the study, all of the orbits are still in the two-dimensional plane even with changes to the RAAN of the orbit. These offsets cause the hyperbolic trajectories to cross paths at certain points as well as continuously increase in range, all of which can be seen in Figs. 12 and 13.

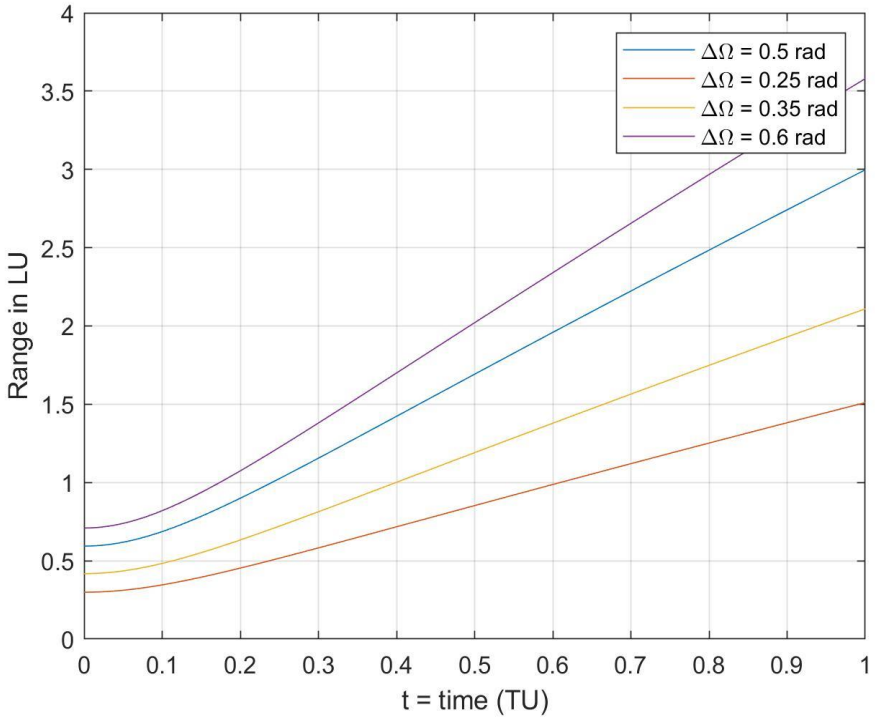

Figure 12. Range vs. Time for Differing Ω

Since the periapsides of the orbits are offset, it makes sense that the relative distance would take on a bucket shape to show how the two orbits curve into or towards each other at the start of the time span before heading in two different directions. It is also not surprising that the range then increases for all RAAN differences since the orbit offsets will cause the separation distance to continuously increase. The rate at which the range increases appears to depend on the size of difference in RAAN with larger values increasing faster than smaller ones.

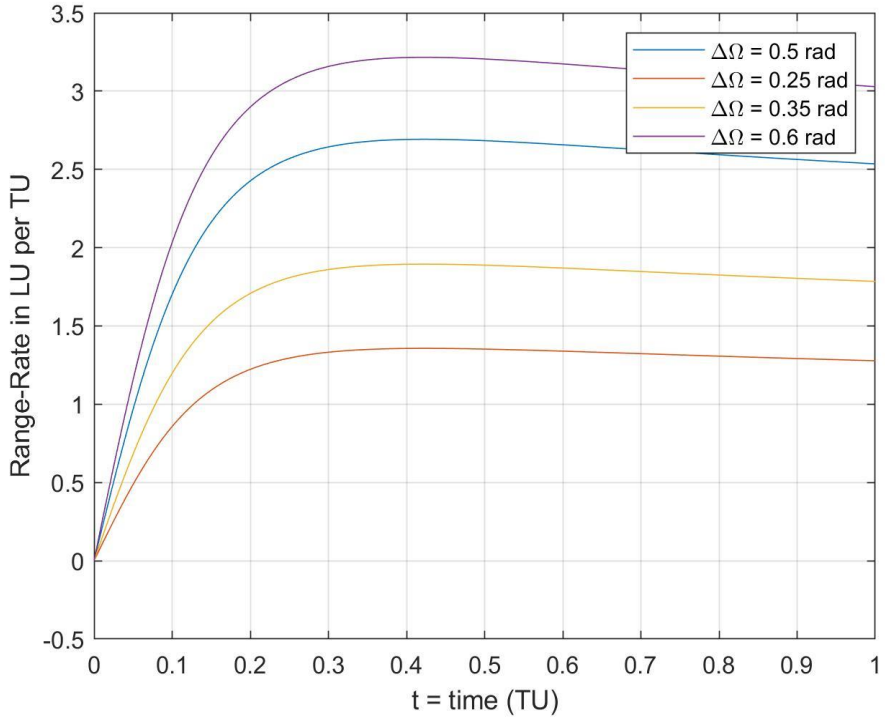

Figure 13. Range-Rate vs. Time for Differing Ω

The range-rate in Fig. 13 appears to show that at a certain point along the time span, a maximum rate is achieved before slightly decreasing back down to an almost steady state. For the most part, all the curves seem to follow the same kind of pattern, with each curve starting at an approximately zero range-rate.

It is also interesting to note that all of the curves appear to be approaching different steady-state values at the end of the time span, once again with larger values of RAAN difference resulting in larger values of steady-state range-rates.

4.4 Spacecraft with Different Positions on Hyperbolas with Differing Inclination

To initiate comparisons, a study of how the range and range-rate would be affected by a position difference and an inclination change was conducted.

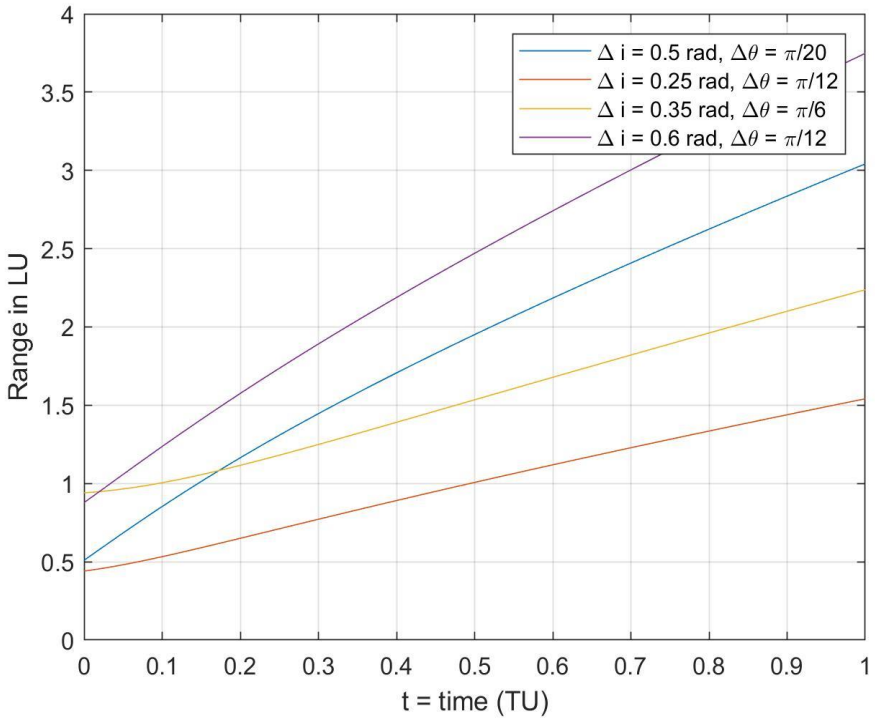

Figure 14. Range vs. Time for Changing Δθ and Differing Inclination

The main difference between Fig. 14 and Fig. 9 is that in Fig. 14 each curve appears to either possess some sort of minimum value of range or start from a value larger than zero. This is due to the curves being shifted by the difference in starting position. Since all of the vehicles are not directly at periapsis and instead maintain some sort of starting separation distance, the curves are still able to follow the same increasing trend present in Fig. 9, but at different rates. The shift in the curves is also able to reveal more information about the trend when the spacecraft do not

start at the same position, which is helpful since it is unlikely that two spacecraft will start from the exact same position on their orbits.

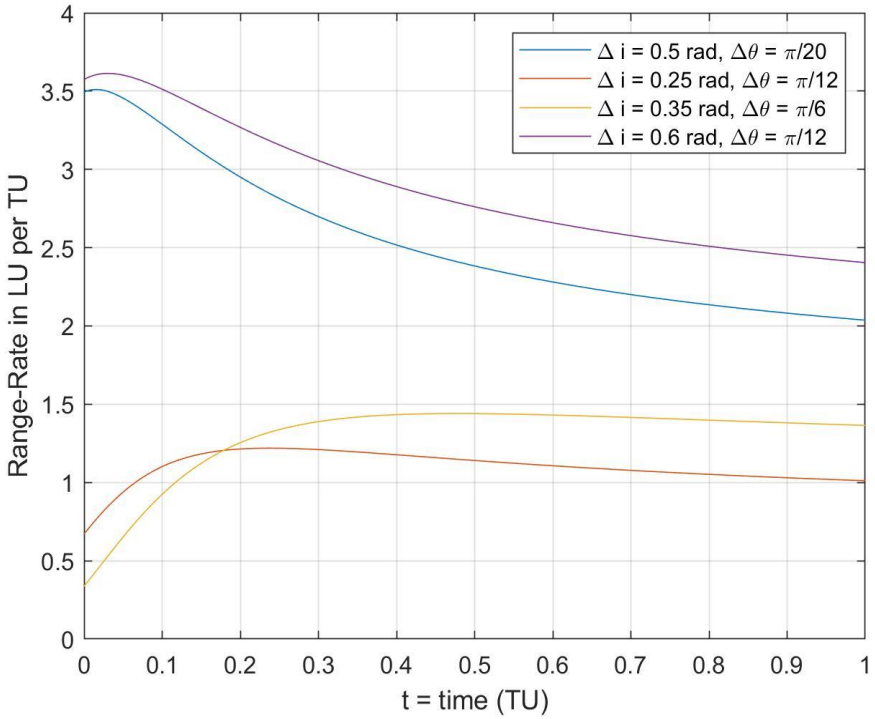

Figure 15. Range-Rate vs. Time for Changing Δθ and Differing Inclination

Similar to the trends present in Fig. 14, Fig. 15 appears to follow the same trends as seen in Fig. 10 but shifted, at least for the $\Delta i = 0.5$ radians and $\Delta i = 0.6$ radians cases. The $\Delta i = 0.35$ radians and $\Delta i = 0.25$ radians cases appear to be the inverse of the original trend in Fig. 10. The peaks and steady states of each curve are much clearer in Fig. 15. Each curve possesses an increase to a maximum value of range-rate before decreasing back down to a steady state condition. It is interesting to note that all of the curves, appear to still have a steady state value that corresponds to their inclination size difference.

4.5 Average Distance and Distance Rate

Table 2. Average Range and Range-Rate for Each Study

Section	**Average Range (LU)**				**Average Range-Rate (LU/TU)**			
Change in Orbital Element	$\Delta = 0.25$	$\Delta = 0.35$	$\Delta = 0.5$	$\Delta = 0.6$	$\Delta = 0.25$	$\Delta = 0.35$	$\Delta = 0.5$	$\Delta = 0.6$
4.2	0.52	0.72	1.02	1.22	1.70	2.38	3.38	4.04
4.3	0.61	0.85	1.20	1.43	1.01	1.41	2.00	2.39
4.4	0.77	1.28	1.38	1.83	1.08	1.11	2.88	3.16

Table 3. Average Range and Range-Rate for Section 4.1

Section	**Average Rate (LU)**				**Average Range-Rate (LU/TU)**			
$\Delta\theta$	$\Delta = \frac{\pi}{20}$	$\Delta = \frac{\pi}{12}$	$\Delta = \frac{\pi}{6}$	$\Delta = \frac{\pi}{2}$	$\Delta = \frac{\pi}{20}$	$\Delta = \frac{\pi}{12}$	$\Delta = \frac{\pi}{6}$	$\Delta = \frac{\pi}{2}$
4.1	0.20	0.60	0.72	2.77	-0.14	-0.41	-0.50	-1.48

Since section 4.1 used one hyperbolic trajectory where the vehicles were placed at different positions whereas the other sections had inclination or RAAN differences in terms of radians, two tables were created to accurately display all the average distances and distance rates.

An interesting observation is that in table 2, sections 4.2 and 4.3 have similar values and trends for the range. This is likely due to both inclination and RAAN causing the spacecraft to have a continuously increasing separation distance. As seen in section 4.4, the offset caused by no longer starting each craft at periapsis appears to cause the average range-rate to decrease

greatly (at least compared to the section 4.2 case) but has an increasing effect on the average range. This could provide a way to minimize the value of the average rate.

When compared to table 2, table 3 shows that when the spacecraft are on the same trajectory, the average range and average range-rate are much easier to manage. The values are almost all smaller than their counterparts, which likely means that when the objects are on the same orbit, they are able to reach their steady state more quickly and at a lower value of range and range-rate.

4.6 Study of Three Spacecraft

A comparison of three spacecraft on two different orbits was conducted to examine the differences in range and range-rate when two vehicles are on the same orbit, but the other is on an orbit with differing RAAN or inclination. An example of how the simulation was setup is shown in Fig. 16, which details that the first and second craft start at periapsis while the third craft is started at a position of 30 degrees ahead of periapsis on the inclined or right ascended orbit. For the purposes of this section, the inclination and RAAN change used was 0.75 radians.

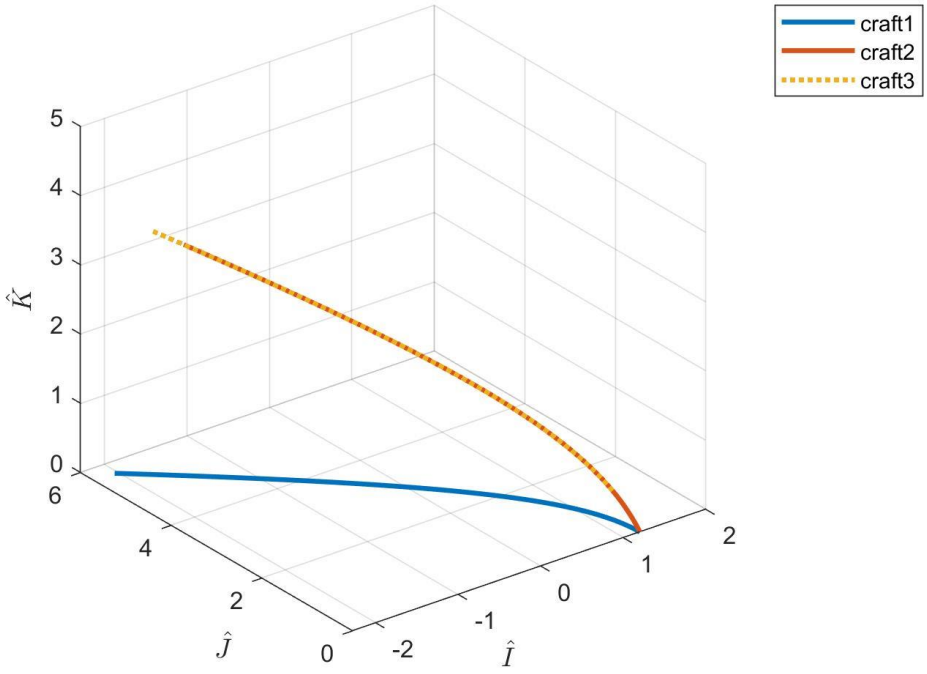

Figure 16. Spacecraft 1,2,3 on Two Differently Inclined Orbits

The distance and distance rates were calculated for each set of two spacecraft (spacecraft 1 to spacecraft 2, spacecraft 1 to spacecraft 3, and spacecraft 2 to spacecraft 3). This enabled a direct comparison to how each spacecraft moved with respect to each spacecraft in the study. These results for a difference in inclination are shown below in Fig. 17 and 18, while the results for a difference in RAAN are shown in Fig. 19 and 20.

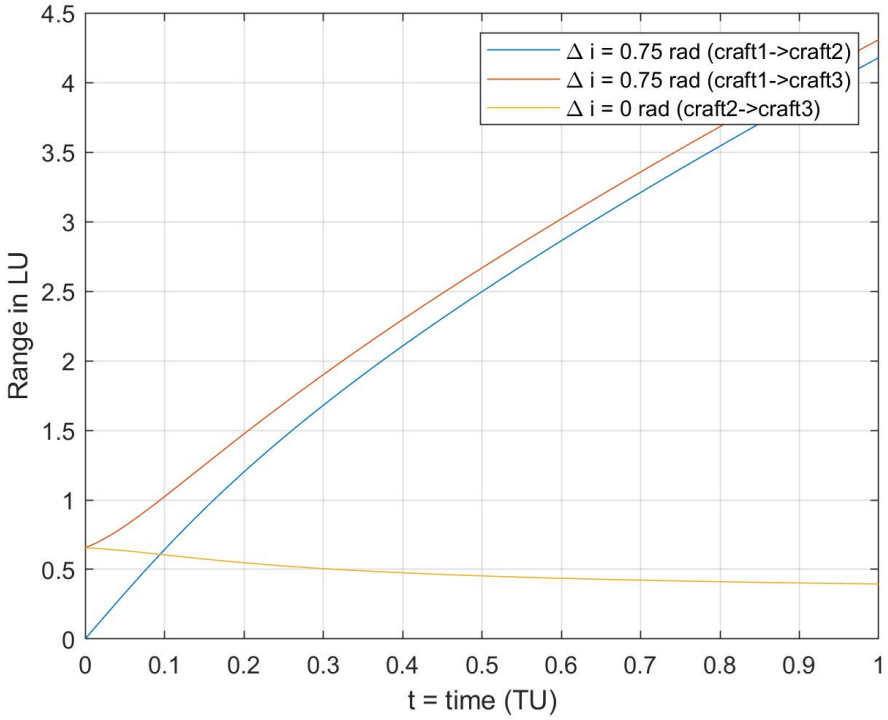

Figure 17. Range of Three Spacecraft on Two Orbits with Differing Inclination

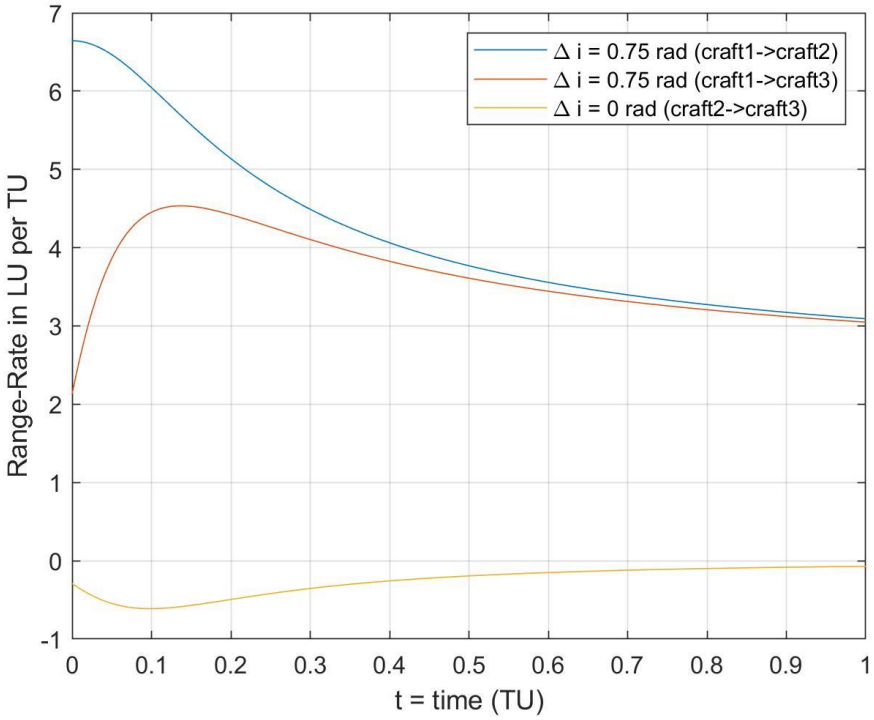

Figure 18. Range-Rate of Three Spacecraft on Two Orbits with Differing Inclination

Since spacecraft 2 and 3 are on the same orbit with a starting separation distance of 30 degrees, it is not surprising that in Fig. 17 and 18, the respective curves maintain a completely different trend than the other curves. The range and range-rate for these two spacecraft also reaches a steady state in both figures where the range and range-rate become practically constant. Again, based on section 4.1, this is expected for spacecraft on the same orbit.

Likewise, it is not surprising that by starting spacecraft 3 at 30 degrees past periapsis with the same inclination difference as spacecraft 2, the steady state of the range-rate between spacecraft 1 and spacecraft 3 winds up being an almost identical value to spacecraft 1 and spacecraft 2. It is however interesting to note that spacecraft 2's range-rate to spacecraft 1 starts out much higher than spacecraft 3's rate to spacecraft 1. This likely has to do with the inclination

change happening immediately upon starting the simulation for spacecraft 2 whereas spacecraft 3 starts already in a plane with different inclination.

Lastly, it can be observed that in Fig. 17 and 18, that the spacecraft 1 and 2 and spacecraft 1 and 3 curves have the same relative trends, but slightly shifted due to the position difference.

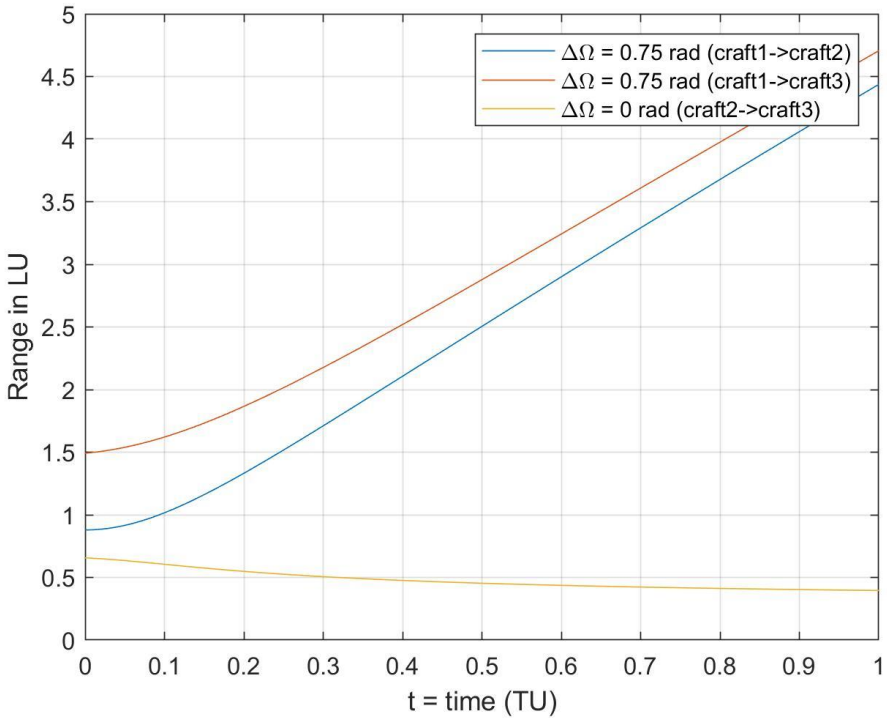

Figure 19. Range of Three Spacecraft on Two Orbits with Differing Ω

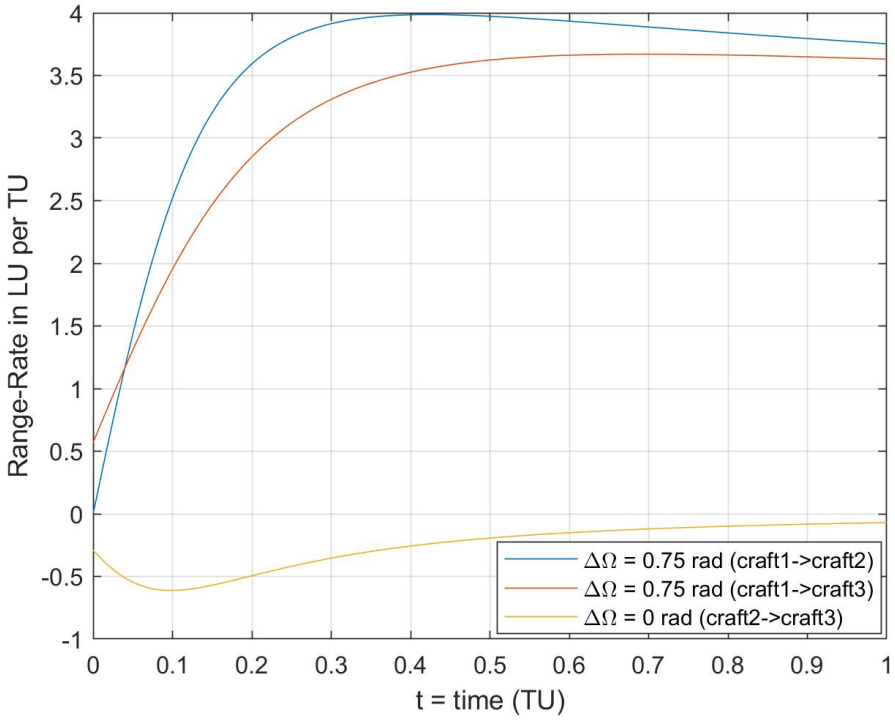

Figure 20. Range-Rate of Three Spacecraft on Two Orbits with Differing Ω

Fig. 19 and 20 produce very similar results to what was reflected in Fig. 17 and 18. However, the spacecraft 1 to spacecraft 2 curve is very similar to the spacecraft 1 to spacecraft 3 curve. Since the RAAN does not add a third dimension to the orbit, this most likely has to do with all of the spacecraft still being in the same plane, thus the curves follow a very similar path to one another only offset by the initial position difference. This is somewhat justified by Fig. 20, where the spacecraft 1 to 3 curve starts out slightly faster than the spacecraft 1 to 2 curve, but then quickly comes to a steady state at an almost identical value of 3.7 LU/TU in about 0.8 TU.

The trends for these two curves are also practically the same in Fig. 19 where the spacecraft 1 to 3 curve starts off at a larger separation than spacecraft 1 to 2, but then immediately takes on almost the same trend as spacecraft 1 to 2 for the entire duration of the

simulation. There is still some difference between the two curves, but this is likely brought on by the fact that there was an initial position difference of 30 degrees between spacecraft 2 and 3.

Finally, just like in Fig. 17 and 18, the spacecraft 2 to 3 curves are expected and showcases that with a RAAN difference, the range and range-rate curves are nearly identical to what they were in the inclination case, which makes sense as nothing about the orbit itself has changed aside from how it was oriented in three-dimensional space. However, it is an interesting observation that the steady state appears to be approximately 0 LU/TU for both Fig. 18 and 20, which shows that eventually the orientations result in the same range-rate for spacecraft in different three-dimensional space with the same two-dimensional characteristics (eccentricity and radius of periapsis).

Table 4. Average Range and Range-Rate for Three Spacecraft on Two Different Orbits with Inclination Difference

Average Range (LU)			**Average Range-Rate (LU/TU)**		
$\Delta i = 0.75$ Craft1→Craft2	$\Delta i = 0.75$ Craft1→Craft3	$\Delta i = 0$ Craft2→Craft3	$\Delta i = 0.75$ Craft1→Craft2	$\Delta i = 0.75$ Craft1→Craft3	$\Delta i = 0$ Craft2→Craft3
1.52	1.82	0.54	5.00	3.82	-0.38

Table 5. Average Range and Range-Rate for Three Spacecraft on Two Different Orbits with RAAN Difference

Average Range (LU)			**Average Range-Rate (LU/TU)**		
$\Delta\Omega = 0.75$ Craft1→Craft2	$\Delta\Omega = 0.75$ Craft1→Craft3	$\Delta\Omega = 0$ Craft2→Craft3	$\Delta\Omega = 0.75$ Craft1→Craft2	$\Delta\Omega = 0.75$ Craft1→Craft3	$\Delta\Omega = 0$ Craft2→Craft3
1.78	2.27	0.54	2.97	2.61	-0.38

For further comparison, tables 4 and 5 were created to highlight the average range and range-rate between each of the different spacecraft cases. As seen in table 4, the average ranges for the spacecraft 1 to spacecraft 2 and 3 cases are both much smaller than the corresponding values in table 5. This is likely because the periapsis' in the RAAN case is offset to start whereas in the inclination case, the periapsis is held constant at the same initial value. As examined in Fig. 17 and 19, the spacecraft 2 to 3 cases for range are practically identical, thus it makes sense that the average range-rate for these cases are approximately the same magnitude.

The most interesting part of the relative rates between tables 4 and 5 is that the range-rate is much larger in value between spacecraft 1 and 2/3 for the inclination case than the RAAN case. This once again likely has to do with the RAAN not bringing in a third dimension. As such, the RAAN only has to deal with the spacecraft moving relative to each other in plane whereas the inclination case has the spacecraft moving away from each other in three components of direction.

Chapter 5

Conclusions and Future Study

5.1 Conclusions

A comparison of different hyperbolic trajectories was explored to find optimal solutions to dealing with a “swarm” of vehicles. By holding radius of periapsis and eccentricity constant, a study of how inclination, RAAN, and three spacecraft on two orbits affect the range and range-rate could be explored. It was determined that two spacecraft on identical orbits revealed the best possible case for minimizing range-rate. When applying an inclination or a RAAN change, the range-rate was drastically increased for all cases. However, the range was actually decreased for certain cases, enabling the possibility to minimize the distance by adjusting the inclination and RAAN of the orbits.

This idea was further explored in section 4.4 where the range-rate was able to be decreased below all the range-rates in section 4.2 by applying both a position and inclination change to the hyperbolic trajectory. This came at the cost of increasing the range between the spacecraft but opens the possibility of minimizing the range-rate for a certain combination of position and orbital element changes. As an advantage, increased distance between spacecraft (with minimum range-rate between them) is an ideal condition for creating a high-resolution distributed sensor.

A further analysis using three spacecraft on two differently oriented orbits was used to reveal unique trends in the way three spacecraft will move relative to each other. It was shown that a change in inclination utilized the smallest range whereas the RAAN could limit the range-

rate between the spacecraft on opposing orbits. When it came to range and range rate of spacecraft on the same orbit, the RAAN produced almost identical results to the inclination change, which proved to be another opportunity where a combination of inclination, RAAN, and position changes may be able to limit both the range and range-rate between all three vehicles.

5.2 Recommendations for Future Study

As a recommendation for future study of the subject, the analytical approximation derived by Willis et al. [4] should be examined. The second-order solution was developed for application to elliptical orbits, but the expansion is not limited to elliptical motion. Further consideration of this approximation as applied to hyperbolic trajectories could reveal a useful tool for the problem considered in this thesis. The numerical calculations are very accurate but will require a high computation time as more spacecraft are considered whereas the analytical approximation is extremely fast, but its accuracy for hyperbolic trajectories needs to be assessed.

It is also suggested that an optimizer for minimizing the average range-rate for some specified range between spacecraft pairs be implemented to determine a way that multiple objects on different orbits can find a time to communicate with each other while they move together around a planet. This would entail coding a method that uses multi-objective optimization, with the objectives being the range-rates of the spacecraft pairs.

Computing a better average of distance and distance rate using weighting is also left as a suggestion. By weighting the largest of the relative values more than the others, one can easily reduce the overall average distance and rate. Likewise, a better weighting scheme that determines a way in which to state which satellite holds more value would inherently provide a

much more accurate average rate and average distance. These values could then be used for better optimization and mission planning.

REFERENCES

[1] Barnhart, D., Vladimirova, T., and Sweeting, M. "Enabling Space Sensor Networks with PCBSat," University of Surrey, 2007.

[2] Edlerman, E., Gurfil, P. "Cluster-Keeping Algorithms for the Satellite Swarm Sensor Network Project," Journal of Spacecraft and Rockets, Vol. 56, No. 3, 2019, doi: 10.2514/1.A34151

[3] Sullivan, J., Grimberg, S. and D'Amico, S. "Comprehensive Survey and Assessment of Spacecraft Relative Motion Dynamics Models," Journal of Guidance, Control, and Dynamics, Vol. 40, No. 8, 2017, pp. 1837-1859, doi: 10.2514/1.G002309

[4] Willis, M., Alfriend, K.T., and D'Amico, S. "Second-order solution for relative motion on eccentric orbits in curvilinear coordinates," Advances in the Astronautical Sciences, Vol. 171, 2020, pp. 767- 790.

[5] Xie, K., Liang, F., Xia, Q., Wang, N., Yuan, H., Liu, X., Wu, Z. "Power Generation on a Bare Electrodynamic Tether During Debris Mitigation in Space," Beijing Institute of Technology, 2021.

[6] Kluever, C. "Spaceflight Mechanics," Encyclopedia of Physical Science and Technology, Vol. 3, 2003, pp. 507-520.

[7] Melton, R. "Approximate Relative Motion Between Hyperbolic Trajectories," The Pennsylvania State University, 2021.

[8] Tapley, B. D., Schutz, B., Born, G. Statistical Orbit Determination. Burlington, MA: Elsevier Academic Press, 2004.

[9] Vallado, D.A., Fundamentals of Astrodynamics and Applications, 2 nd ed. El Segundo, CA: Microcosm Press, 2001.

[10] Prussing, J.E. and Conway, B.A., Orbital Mechanics, 2nd ed., Oxford University Press, New York – Oxford, 2013.

[11] Vasile, M., "A Global Approach to Optimal Space Trajectory Design," Advances in Astronautical Sciences, Vol. 114, 2003, pp. 621-640.

[12] Mathworks, ODE45 Documentation. [Online] Available: https://www.mathworks.com/help/matlab/ref/ode45.html.

Clifford Stueck

EDUCATION

Bachelor of Science in Aerospace Engineering (Expected Graduation: May 2022)
Master of Science in Aerospace Engineering (Expected Graduation: May 2023)
The Pennsylvania State University, University Park, PA

Minors: Information Science Technology
Engineering Mechanics

- College of Engineering
- Schreyer Honors College

SOFTWARE

SolidWorks (CSWP), C++, MATLAB, SQL, Java, LaTeX, Microsoft Office, HTML/CSS

WORK EXPERIENCE

- **Pratt & Whitney,** East Hartford, CT (May 2021 - Aug 2021) *Summer Intern*
  - Focused on Class 1 and Class 2 changes for the PW1500G and PW1900G engine nacelle
  - Reviewed, created, and modified nacelle hardware changes to the thrust reverser, fan cowl, and inlet systems—keeping Collins Aerospace updated on current engine design

RESEARCH

- **Orbital Mechanics Research** (April 2021 - May 2022)
  - Research to further assess and study the accuracy of the relative motion model applied to hyperbolic paths
  - Thesis will examine accuracy in the presence of perturbing forces and verify existing second order solutions using another form of approximation for comparison

INTERESTS & INVOLVEMENT

- **Penn State Racing Formula SAE,** *Chassis Lead* (Aug 2018 - Present)
  - Apply engineering coursework, communication skills, and budget management expertise to design and manufacture a formula-style race car
  - Manufacture and post-process negative molds for diffuser, nosecone, carbon fiber wings, and side pods
  - Lay up carbon fiber, honeycomb, and structural adhesive for monocoque
  - Use CAD to design chassis and other ancillary components
- **Engineering Ambassadors at Penn State,** *Member* (March 2019 - Present)
  - Conduct engineering outreach visits at K-12 schools
  - Generate awareness of Engineering as a potential career among secondary school students
- **Engineering Student Tours and Resources,** *Director of Recruitment* (Jan 2020 - Present)
  - Founding member of new organization consisting of select students and Penn State Engineering faculty focused on raising profile of Penn State Engineering
  - Provide tours & presentations to prospective & accepted College of Engineering students
- **Engineering Study Abroad** in Pforzheim Germany, Student (May 2019 - July 2019)
  - Successfully completed three classes focused on industrial engineering and manufacturing
  - Toured Audi, Mercedes, and Porsche manufacturing plants

ACADEMIC HONORS

- Dean's List (Fall 2018 – Present)
- Tau Beta Pi - The Engineering Honor Society
- Sigma Gamma Tau – National Aerospace Engineering Honor Society
- Certified SolidWorks Professional